Supporting Information

Machine learning identifies ecological selectivity patterns across the end-Permian mass extinction

William J. Foster[a,b,c], Georgy Ayzel[b], Jannes Münchmeyer[d,e], Tabea Rettelbach[f,e,b], Niklas Kitzmann[g], Terry T. Isson[h], Maria Mutti[b], Martin Aberhan[a]

[a] Museum für Naturkunde, Leibniz Institute for Evolution and Biodiversity Science, Berlin, Germany.

[b] Universität Potsdam, Institute for Geosciences, Potsdam-Golm, Germany.

[c] Universität Hamburg, Institute für Geologie, Hamburg, Germany.

[d] GFZ German Research Centre for Geoscience, Potsdam, Germany.

[e] Humboldt-Universität zu Berlin, Department of Computer Science, Berlin, Germany.

[f] Alfred Wegener Institute Helmholtz Center for Polar and Marine Research, Potsdam, Germany.

[g] Potsdam Institute for Climate Impact Research (PIK)—Member of the Leibniz Association, Potsdam, Germany.

[h] University of Waikato, School of Science, Tauranga, New Zealand.

Corresponding Author: William Foster, w.j.foster@gmx.co.uk

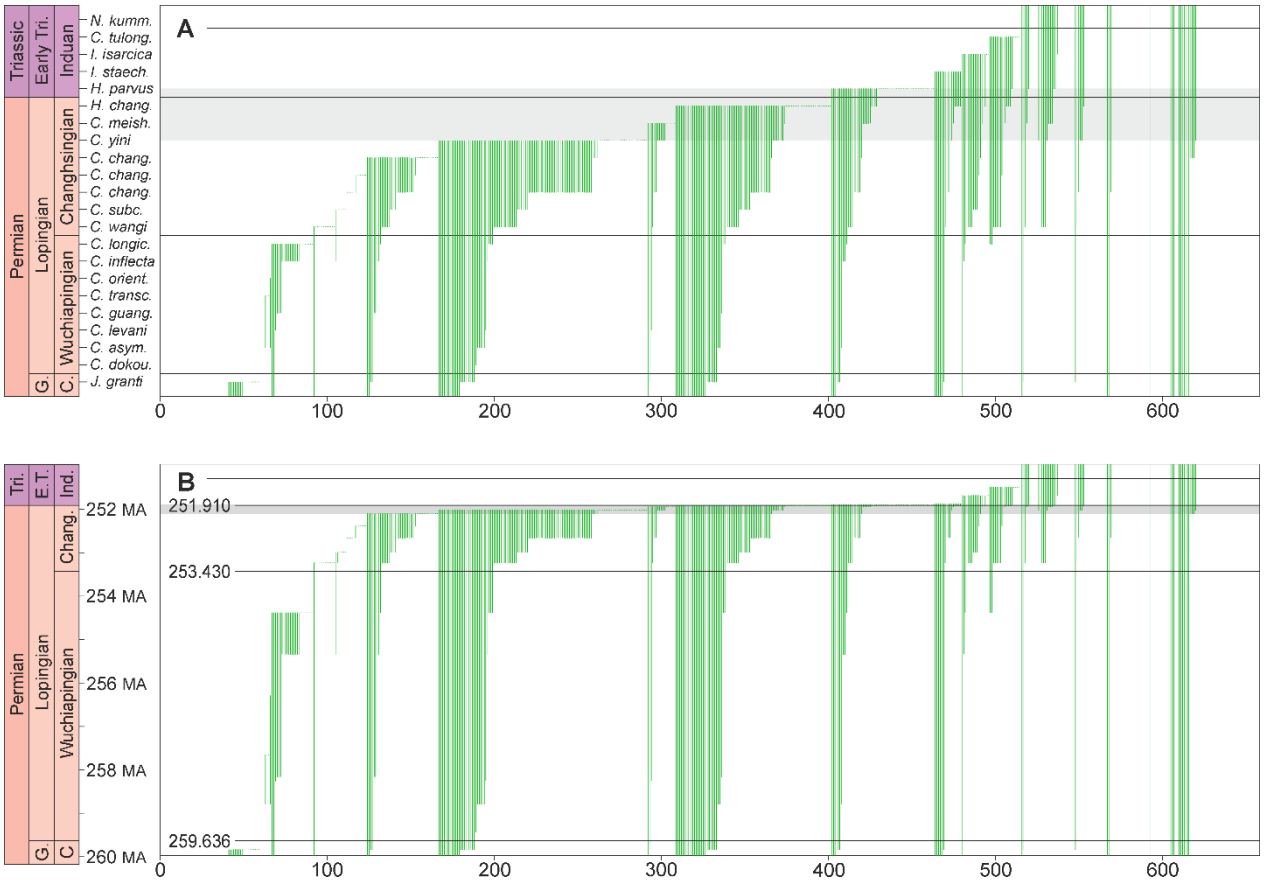

Figure S1. Stratigraphic ranges of fossil marine taxa used in this study. Genus numbers are shown on the x axis and are organized by the last appearance date (LAD). The extinction interval is highlighted in gray. Substage and stage boundaries are shown by horizontal black lines. A) Genus ranges scaled to conodont zones with each conodont zone given an equal thickness. G. = Guadalupian, Early Tri. = Early Triassic, C. = Capitanian. Conodont zones after Yuan et al. (2014), Jin et al. (2003) and Zhang et al. (2007): *C. dokou*. = *Clarkina dukouensis*, *C. asym*. = *C. asymmetrica*, *C. guang*. = *C. guangyuanensis*, *C. transc*. = *C. transcaucasia*, *C. orient*. = *C. orientalis*, *C. longic*. = *C. longicuspida*, *C. subc*. = *C. subcarinata*, *C. chang*. = *C. changxingensis*, *C. meish*. = *C. meishanensis*, *H. chang*. = *Hindeodus changxingensis* – *C. zhejiangensis*, *I. staech*. = *Isarcicella staeschei*, *C. tulong*. = *C. tulongensis* – *C. planata*, *N. kumm*. = *Neogondolella kummeli* – *N. krystyni*. B) Genus ranges scaled to radiometric dates. Radiometric dates after Burgess et al. (2014) and Yuan et al. (2014). Tri = Triassic, E.T. = Early Triassic, Chang. = Changhsingian. MA = million years before present.

Extended Materials and Methods

The body size of each species was based on the reported sizes, or taken from figured specimens, and the maximum body size for the species with the most occurrences within a genus was taken to represent the genus' body size. The geometric mean of the genus body size was then calculated following Jablonski (1996). Because most genera that span the Permian/Triassic boundary are thought to have adapted their body size in response to environmental changes (Twitchett 2007), and because interpopulation variance is not captured by single measurements for each genus, body size was categorized into three semi-quantitative groups (Table 1). The carbonate load was calculated by multiplying the body size of each genus that precipitates a carbonate skeleton by the percentage of the ash-free dry mass to the total mass for each faunal group based on modern representatives. Genera that do not possess a carbonate skeleton, e.g., radiolarians, were categorized as having no carbonate load. Ornamentation is a factor that is commonly related to predation pressure, whereby strong ornamentation enhances resistance against shell-breaking (Aberhan et al. 2006). In this study, however, we include ornamentation as an ecological attribute that is also related to carbonate load, whereby genera with strongly ornamented calcareous shells are expected to have greater carbonate loads than smooth genera. To investigate bathymetric range, each occurrence was classified into one of four broad depositional settings: littoral, platform, slope, basin, and unknown. The bathymetric range is then calculated for each taxon based on the number of environments it occurs in from the shallowest setting to the deepest settings. E.g., if a genus occurred in littoral to basin settings it was classified as "4", whereas a genus only found in basinal depositional settings would be classified as "1". Respiratory proteins are variable in structure, oxygen affinity, and concentration among invertebrate groups (Herreid II 1980). Because of the different responses of proteins to changes in pH, temperature, and salinity it is expected that invertebrates with certain pigments, such as hemerythrin, will be less impacted by hypoxia than invertebrates that do not possess this pigment as an oxygen carrier. This selectivity pattern has been suggested to explain why lingulid brachiopods flourished following the end-Permian mass extinction (Peng et al. 2007; Posenato et al. 2014). Variances in the respiratory protein are known between invertebrate groups, but the variance within classes, such as bivalves, is less well-known.

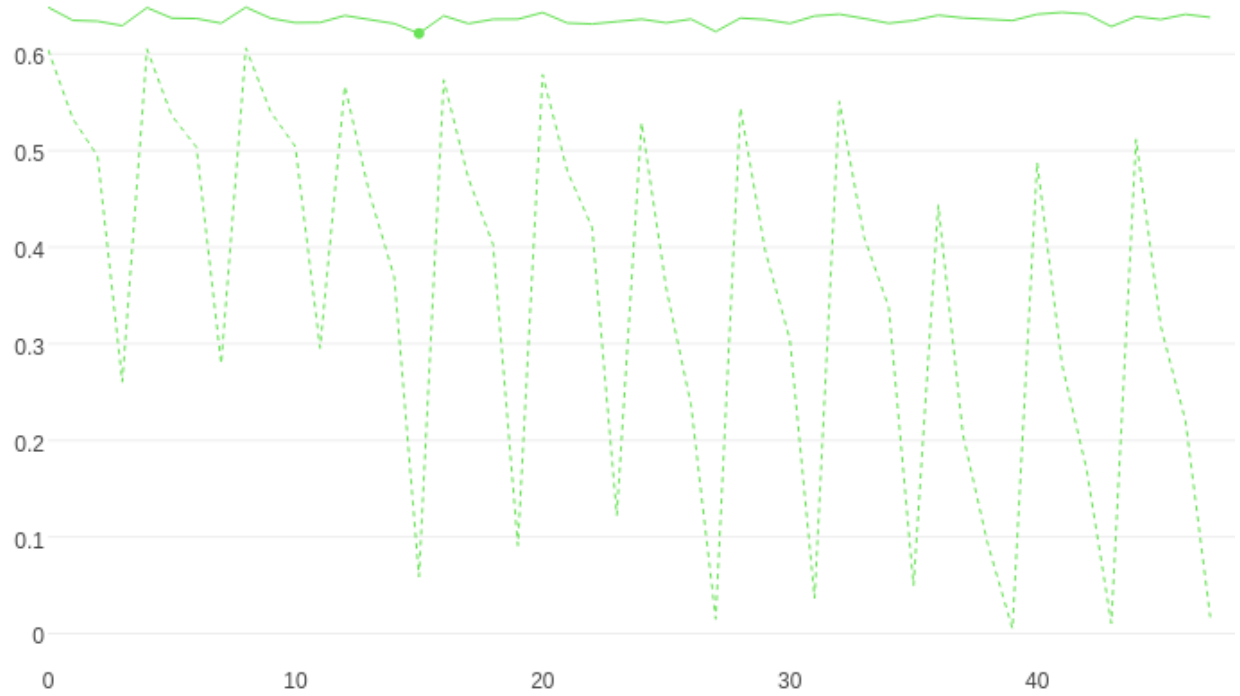

Figure S2. Performance of the machine learning algorithm evaluated on testing (solid) and training (dashed) data, expressed as cross-entropy loss (log loss) for 48 different learner hyperparameter sets. The corresponding hyperparameters for each run are given in Table S1.

Table S1. Machine learning algorithm hyperparameter sets evaluated in Fig. S2.

Run number	Learning rate	l2 leaf regularization	Tree depth
1	0.001	1	2
2	0.005	1	2
3	0.01	1	2
4	0.1	1	2
5	0.001	3	2
6	0.005	3	2
7	0.01	3	2
8	0.1	3	2
9	0.001	5	2
10	0.005	5	2
11	0.01	5	2
12	0.1	5	2
13	0.001	1	4
14	0.005	1	4
15	0.01	1	4
16	0.1	1	4
17	0.001	3	4
18	0.005	3	4
19	0.01	3	4
20	0.1	3	4
21	0.001	5	4
22	0.005	5	4
23	0.01	5	4
24	0.1	5	4

Run number	Learning rate	l2 leaf regularization	Tree depth
25	0.001	1	6
26	0.005	1	6
27	0.01	1	6
28	0.1	1	6
29	0.001	3	6
30	0.005	3	6
31	0.01	3	6
32	0.1	3	6
33	0.001	5	6
34	0.005	5	6
35	0.01	5	6
36	0.1	5	6
37	0.001	1	10
38	0.005	1	10
39	0.01	1	10
40	0.1	1	10
41	0.001	3	10
42	0.005	3	10
43	0.01	3	10
44	0.1	3	10
45	0.001	5	10
46	0.005	5	10
47	0.01	5	10
48	0.1	5	10

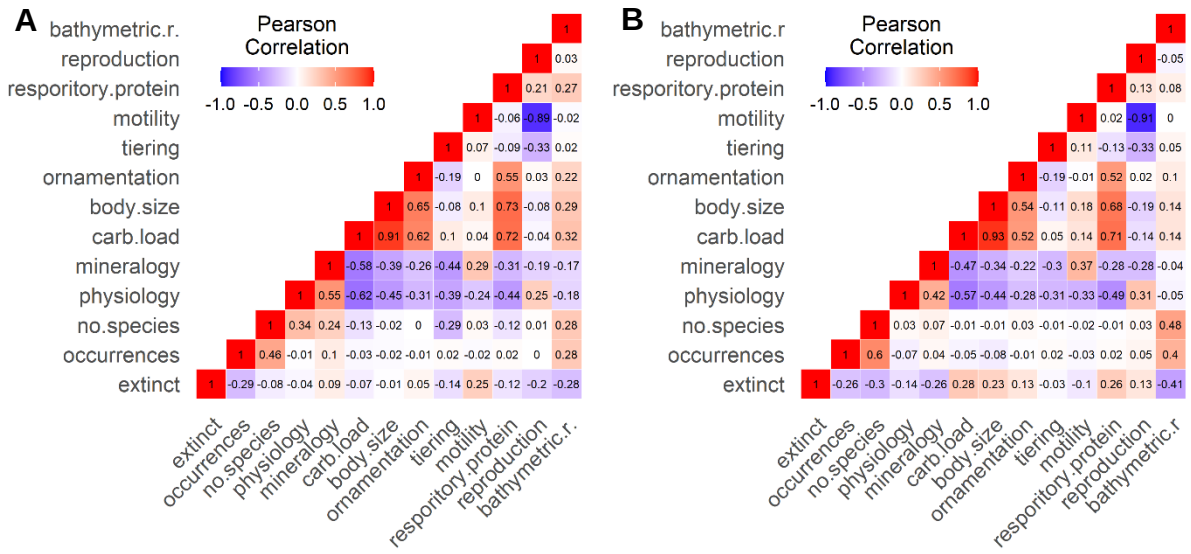

Figure S3. Correlation matrix of the investigated variables of each taxon during (A) the extinction interval, and (B) pre-extinction Changhsingian.

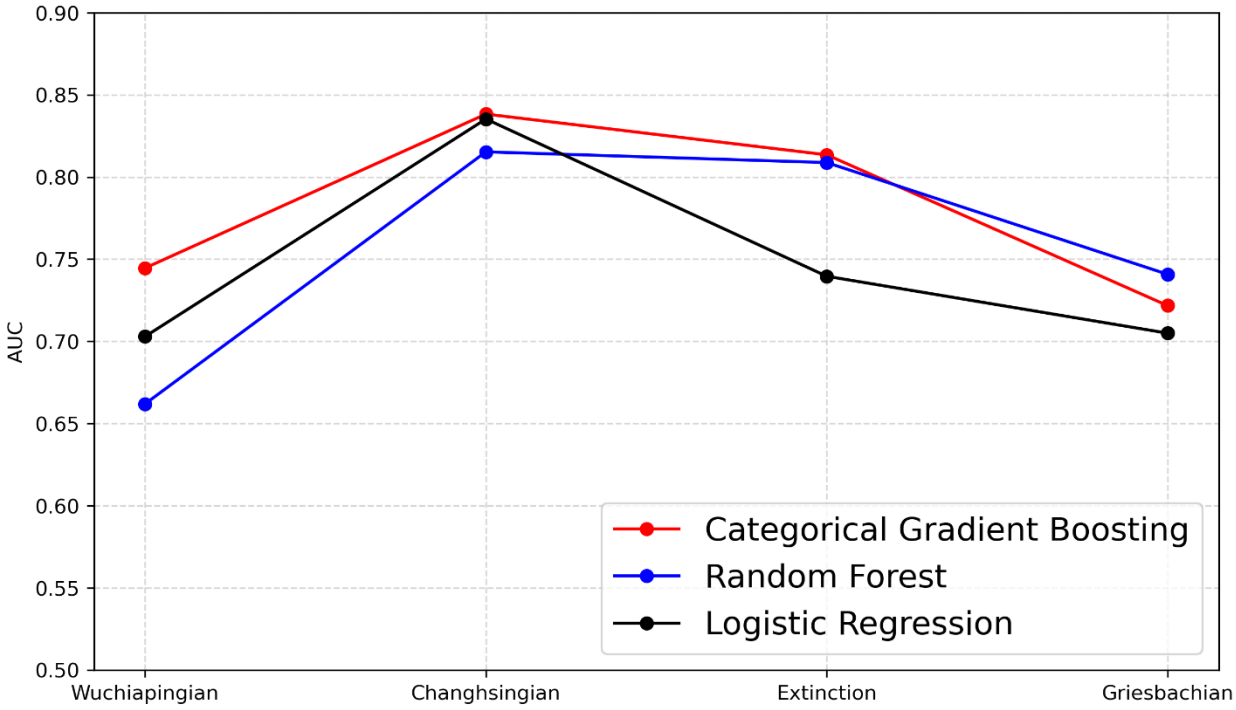

Figure S4. Comparison of the average AUC scores between the Catboost, Random Forest, and Logistic regression algorithms.

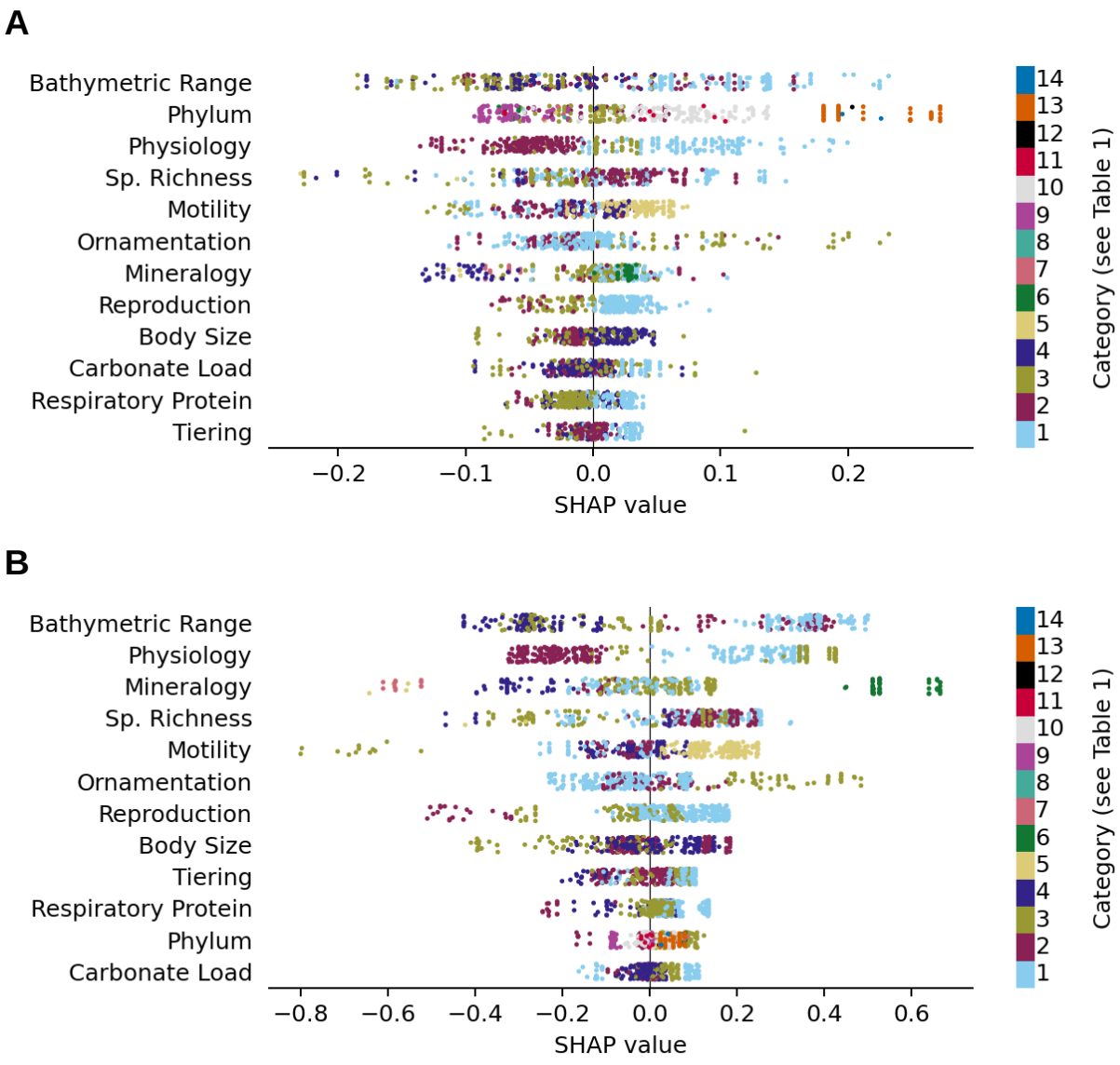

Figure S5. SHAP summary plot for the extinction interval using the Random Forest algorithm (A) and Catboost algorithm (B) showing how the different values of each ecological attribute effect the model predictions for the extinction interval. The horizontal location of the values shows whether a data point from the training dataset is associated with a higher or lower prediction. The vertical position corresponds to the relative importance of each ecological attribute. The SHAP summary plot for split 5 during the extinction interval is shown. Note the small range in SHAP values for each feature in the Random Forest algorithm, especially when compared to the Catboost method.

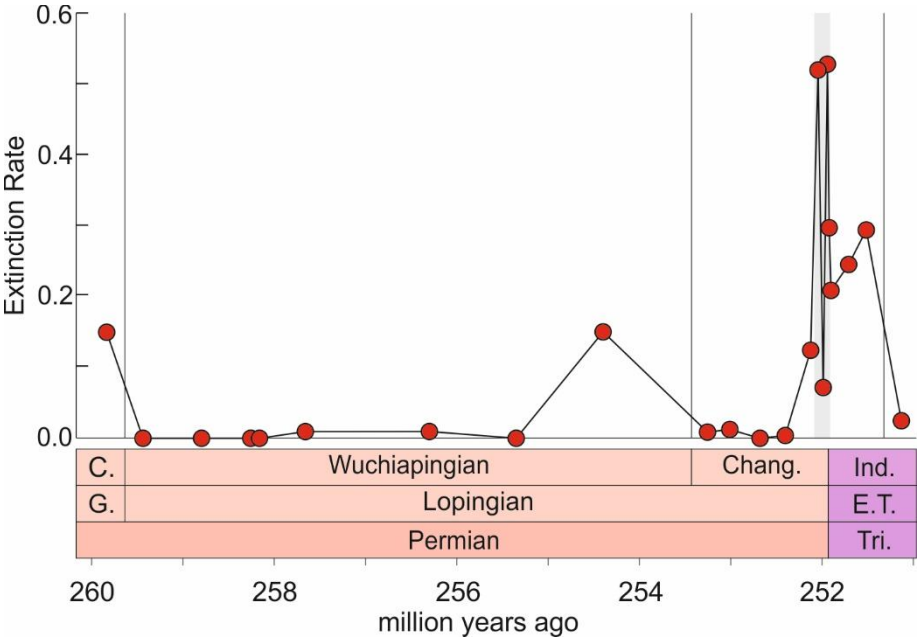

Figure S6. High-resolution regional extinction rates of marine genera across the studied interval in South China. Extinction rates are calculated after Foote (2000). The extinction interval is highlighted in grey after Wang et al. (2014). Radiometric ages after Burgess et al. (2014) and Yuan et al. (2014). Conodont zones after Yuan et al. (2014) See Figure 1 to zoom in on extinction rates across the Permian-Triassic boundary interval. C. = Capitanian, G. = Guadalupian. E.T. = Early Triassic, Ind. = Induan, Tri. = Triassic, Chang. = Changhsingian.

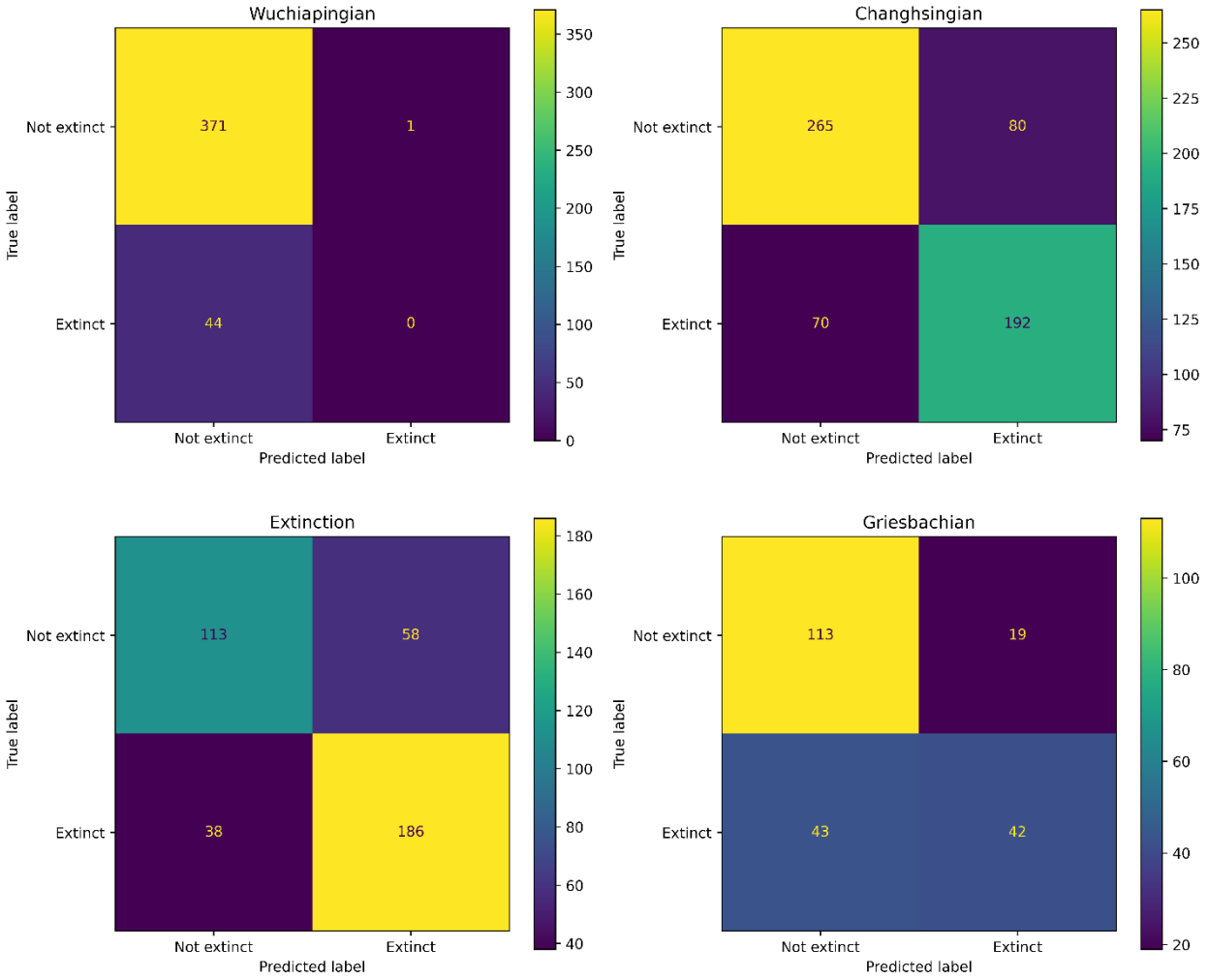

Figure S7. Confusion matrix plots for the CatBoost for each investigated time interval. These plots are based on a probability of 0.5, i.e., a genus is classified as extinct if the predicted probability is over 0.5.

Table S2. Relative importance of ten ecological traits and two phylogenetic attributes of marine genera for predicting extinction risk across the end-Permian mass extinction using high performance categorical gradient boosting on decision trees.

Wuchiapingian	Feature Importance	**Changhsingian**	Feature Importance
Bathymetric Range	26.38	Bathymetric Range	24.35
Phylum	8.96	Sp. richness	15.50
Sp. richness	8.49	Carbonate load	9.66
Mineralogy	7.51	Respiratory protein	8.65
Body size	6.85	Body size	7.32
Ornamentation	6.55	Tiering	6.85
Tiering	6.43	Mineralogy	5.50
Carbonate load	6.38	Ornamentation	5.22
Respiratory protein	6.22	Physiology	5.37
Physiology	6.16	Reproduction	4.30
Motility	5.15	Motility	4.00
Reproduction	4.91	Phylum	3.29

Extinction Interval	Feature Importance	**Griesbachian**	Feature Importance
Bathymetric Range	14.54	Tiering	10.98
Mineralogy	11.51	Mineralogy	10.88
Sp. richness	11.07	Bathymetric Range	9.96
Physiology	10.79	Ornamentation	8.80
Ornamentation	8.39	Reproduction	8.19
Body Size	8.08	Carbonate load	7.99
Motility	7.30	Physiology	7.71
Reproduction	7.22	Sp. richness	7.70
Carbonate Load	5.83	Motility	7.54
Tiering	5.24	Body size	7.28
Phylum	5.06	Phylum	6.91
Respiratory protein	4.93	Respiratory protein	6.07

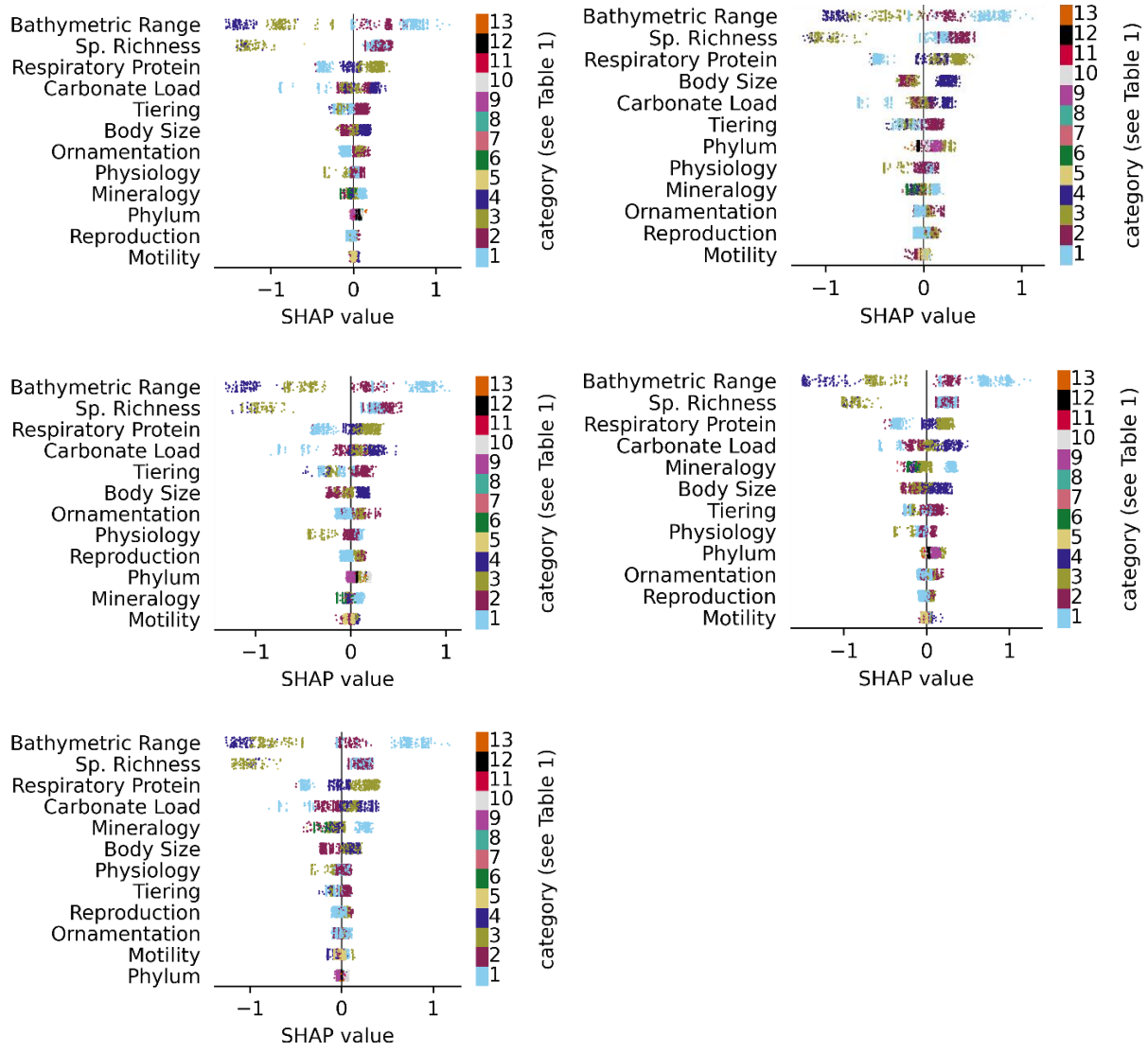

Figure S8. SHAP summary plots showing the relative importance of ecological attributes and how the different values for each ecological category affect the model predictions for the Changhsingian. The horizontal location of the values shows if a data point from the training dataset is associated with a higher or lower prediction. The points are colored according to the categorical value given in Table 1 for each feature.

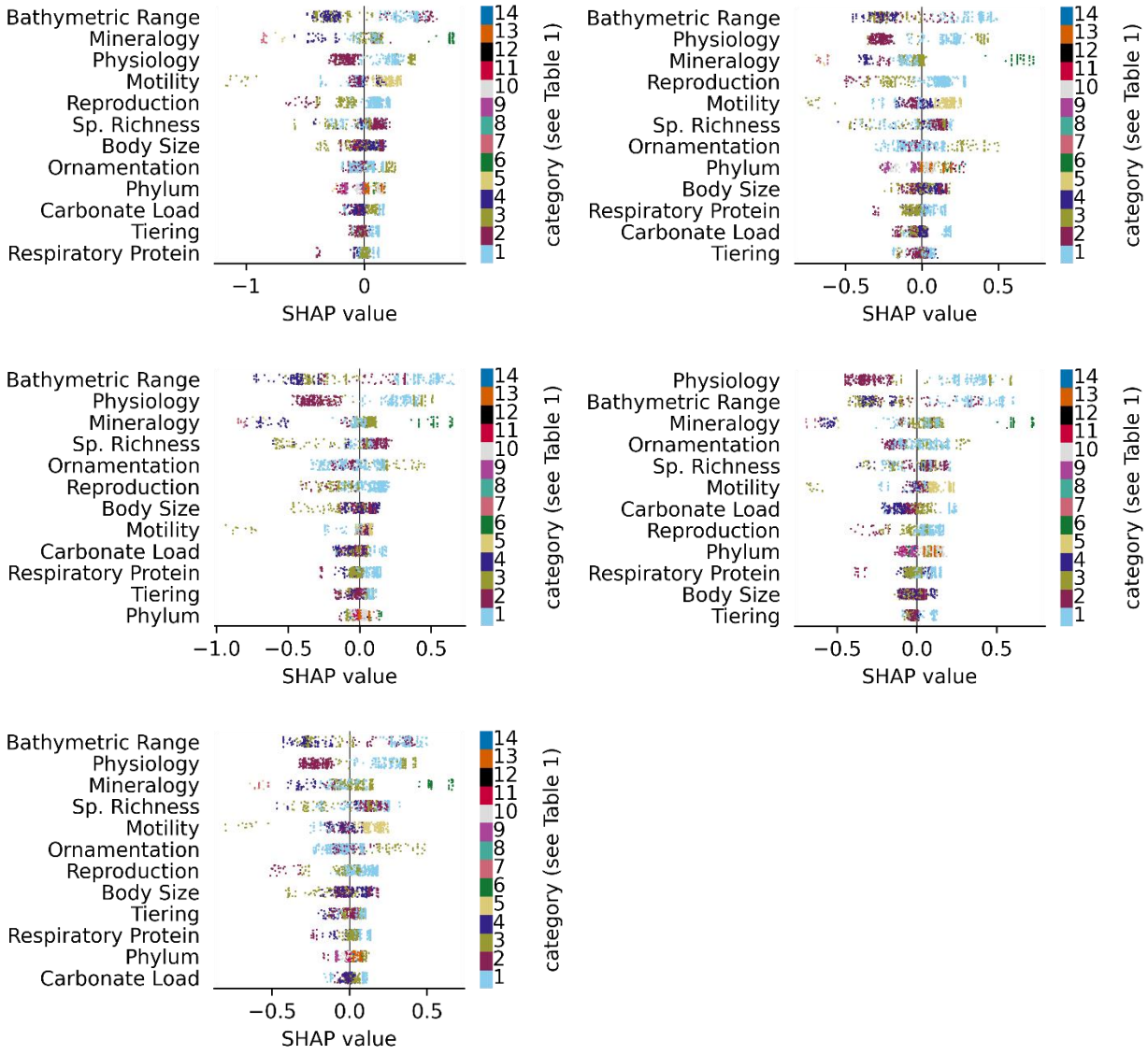

Figure S9. SHAP summary plots showing the relative importance of ecological attributes and how the different values for each ecological category affects the model predictions for the Extinction Interval. The horizontal location of the values shows if a data point from the training dataset is associated with a higher or lower prediction. The points are colored according to the categorical value given in Table 1 for each feature.

References

Aberhan, M., Kiessling, W., and Fürsich, F.T. 2006. Testing the role of biological interactions in the evolution of mid-Mesozoic marine benthic ecosystems. Paleobiology 32:259-277.

Burgess, S.D., Bowring, S.A., and Shen, S-Z. 2014. High-precision timeline for Earth's most severe extinction. Proceedings of the National Academy of Sciences 111:5060-5060.

Foote, M. 2000. Origination and extinction components of taxonomic diversity: general problems. Paleobiology 26:74-102.

Herreid II, C.F. 1980, Hypoxia in Invertebrates. Comp. Biochem. Physiol 67A:311-320.

Jablonski, D. 1996. in D, Jablonski., D.H. Erwin., J, Lipps., (eds). Evolutionary Paleobiology. Chicago Press, 256-289.

Jin, Y.G., Henderson, C.M., Wardlaw, B.R., Shen, S.Z., Wang, X.D., Wang, Y., Cao, C.Q. and Chen, L. 2003. Proposal for the Global Stratotype Section and Point (GSSP) for the Guadalupian-Lopingian Boundary. Permophiles 39:32-42.

Knoll, A.H., Bambach, R.K., Payne, J.L., Pruss, S., and Fischer, W.W. 2007. Paleophysiology and end-Permian mass extinction. Earth and Planetary Science Letters 256:295-313.

Peng, Y., Shi, G.R., Gao, Y., He, W., and Shen, S-Z. 2007. How and why did the Lingulidae (Brachiopoda) not only survive the end-Permian mass extinction but also thrive in its aftermath? Palaeogeography, Palaeoclimatology, Palaeoecology 252:118-131.

Posenato, R., Holmer, L.E., Prinoth, H. 2014. Adaptive strategies and environmental significance of lingulid brachiopods across the late Permian extinction. Palaeogeography, Palaeoclimatology, Palaeoecology 399:373-384.

Ries, J.B. 2011. Physicochemical framework for interpreting the biological calcification response to CO2-induced ocean acidification. Geochimica et Cosmochimica Acta 75:4053-4064.

Twitchett, R.J. 2007. The Lilliput effect in the aftermath of the end-Permian extinction event. Palaeogeography, Palaeoclimatology, Palaeoecology 252:132-144.

Wang, Y., Sadler, P.M., Shen, S.Z., Erwin, D.H., Zhang, Y.C., Wang, X.D., Wang, W., Crowley, J.L. and Henderson, C.M. 2014. Quantifying the process and abruptness of the end-Permian mass extinction. Paleobiology 40:113-129.

Yuan, D.X., Shen, S.Z., Henderson, C.M., Chen, J., Zhang, H. and Feng, H.Z. 2014. Revised conodont-based integrated high-resolution timescale for the Changhsingian Stage and end-Permian extinction interval at the Meishan sections, South China. Lithos 204:220-245.

Zhang, K., Tong, J., Shi, G.R., Lai, X., Yu, J., He, W., Peng, Y. and Jin, Y. 2007. Early Triassic conodont – palynological biostratigraphy of the Meishan D Section in Changxing, Zhejiang Province, South China. Palaeogeography, Palaeoclimatology, Palaeoecology 252:4-23.